J. Fluid Mech. (1990), *vol.* 217, *pp.* 71–91
Printed in Great Britain

Capillary–gravity Kelvin–Helmholtz waves close to resonance

By V. BONTOZOGLOU† AND T. J. HANRATTY
Department of Chemical Engineering, University of Illinois at Urbana-Champaign, Urbana, IL 61801, USA

(Received 2 September 1988 and in revised form 2 January 1990)

Capillary–gravity waves of permanent form at the interface between two unbounded fluids in relative motion are considered. The range of wavelengths for an internal resonance with the second harmonic and a period-doubling bifurcation are found to depend on the current speed. The Kelvin–Helmholtz instability of short waves becomes strongly subcritical near resonance. It is speculated that this instability is needed to trigger a period-doubling bifurcation. This notion is used to explain the development of waves at short fetch and the initiation of liquid slugs for gas–liquid flow in a horizontal pipe.

1. Introduction

Capillary–gravity waves of permanent form at the interface between two unbounded fluids in relative motion (Kelvin–Helmholtz waves) are considered. Attention is focused on wavelengths in the range where the second harmonic of a wave with infinitesimal amplitude resonates with the fundamental. The effect of current speed is examined both analytically and numerically and the weakly nonlinear Kelvin–Helmholtz instability is studied, for the first time, in this range of wavelengths.

Kelvin–Helmholtz (K–H) gravity waves have been considered by Maslowe & Kelly (1970), Saffman & Yuen (1982), Pullin & Grimshaw (1983), Miles (1986) and Bontozoglou & Hanratty (1988) and gravity–capillary waves by Drazin (1970), Nayfeh & Saric (1972) and Weissman (1979). Saffman & Yuen (1982) showed, for gravity waves in unbounded fluids, that the nonlinear K–H instability is always supercritical (i.e. the critical velocity, U_c, beyond which waves of a given amplitude cease to exist is an increasing function of the wave amplitude). Miles (1986) and Bontozoglou & Hanratty (1988) showed that for some finite fluid depths the K–H instability for gravity waves can become subcritical (i.e. U_c is a decreasing function of the wave amplitude). Nayfeh & Saric (1972) have pointed out that the inclusion of surface tension can make the instability subcritical for small enough wavelengths, even for unbounded fluids. Miles (1986) considered capillary–gravity waves at the interface of fluids of finite depths and noted the need for reformulating the problem in the neighbourhood of the resonant wavelength, where his results were no longer valid.

Capillary–gravity waves with wavelengths close to the resonance condition have been considered only for free-surface waves. Wilton (1915), revoking Stokes hypothesis, obtained two solutions for dimensionless surface tension κ equal to $\frac{1}{2}$.

† Present address: Chemical Process Engineering Research Institute, PO Box 19517, 54006 Thessaloniki, Greece.

Pierson & Fife (1961) extended Wilton's solutions in the neighbourhood of $\kappa = \frac{1}{2}$. Chen & Saffman (1979, 1980) interpreted Wilton's ripples as a bifurcation phenomenon by which a wave doubles its wavelength ($2 \rightarrow 1$ bifurcation) and defined, both analytically and numerically, a more general class of bifurcations. Schwartz & Vanden-Broeck (1979) calculated families of capillary–gravity waves at a free surface, and Vanden-Broeck (1980) demonstrated that similar waves exist at an interface between two stationary fluids of different densities.

The effect of the current velocity U on resonance, on period-doubling bifurcation and on the existence of progressive waves of permanent form is examined in the present paper. For small amplitude waves, algebraic expressions are derived using a weakly nonlinear approximation. A numerical method based on the hodograph formulation by Saffman & Yuen (1982) is used to obtain results for larger waves and, in particular, to obtain an understanding of the $2 \rightarrow 1$ bifurcation.

The range of wavelengths over which internal resonance with the second harmonic is important is shown to depend strongly on the current speed U; for certain values of U, resonance is significant only extremely close to a singular wavelength and the Stokes-type expansion is valid everywhere else.

The period-doubling bifurcation, discovered by Chen & Saffman (1979, 1980) for free-surface waves, is found to depend dramatically on the current speed. There is encouraging agreement between the numerical analysis presented in this paper and the bifurcation discovered in experiments by Choi (1977). This period-doubling has been documented in several papers (Choi 1977; Ramamonjarisoa, Baldy & Choi 1978; Kawai 1979) and could constitute an important step in the evolution of wind ripples.

The existence of waves of permanent form in the neighbourhod of the K–H instability is also examined. An interesting new result is that, for wavelengths shorter than the resonant and approaching it (capillary-side waves), the Kelvin–Helmholtz instability becomes increasingly subcritical. The second family (gravity-side waves) shows a more complicated dependence of the critical current speed on wave steepness in that it reaches a maximum for waves of intermediate height.

These results on the existence of waves of permanent form are applied to the question of how the $2 \rightarrow 1$ bifurcation is triggered. It is speculated that the bifurcation takes place when the waves become Kelvin–Helmholtz unstable, a notion which seems consistent with the range of wind velocities under which the phenomenon has been observed experimentally.

Experimental results of Andritsos, Williams & Hanratty (1989) (for co-current flow of air and water–glycerine mixtures of varying viscosity) are compared with a prediction based on the notion that slugs form from the bifurcation and further growth of capillary–gravity ripples. This interpretation seems to explain the initiation of slugs in viscous liquids. It could also be of speculative interest for gas/water flows in large diameter pipes (where the presently used theory of instability of long wavelength disturbances gives unreasonably large predictions for the critical gas velocity).

In §2 the mathematical formulation of the problem is given. The weakly nonlinear approximation is developed in §3 and results are presented in §4. The numerical method is developed in §5 and used to calculate the bifurcation locus in §6. The Kelvin–Helmholtz instability and its speculated role in triggering the bifurcation are discussed in §7. The discussion of the onset of slugging is given in §8.

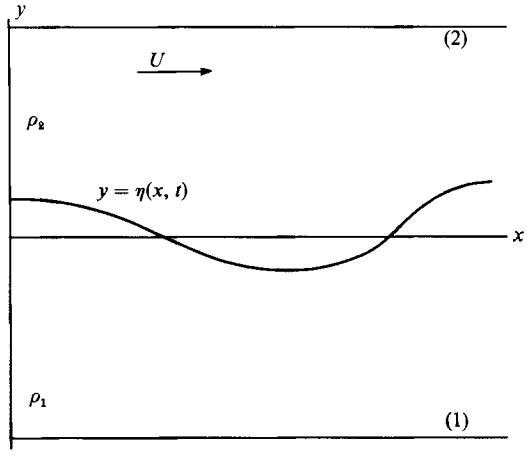

FIGURE 1. Sketch of flow system.

2. Problem formulation – previous results

Periodic waves at the interface between two unbounded fluids are considered. The fluids have different densities and the upper is moving relative to the lower with a horizontal velocity U. They are incompressible and inviscid; the motion is assumed to be irrotational. Solutions are obtained for two-dimensional, periodic waves of permanent form whose wavelength, L, is such that both gravity and surface tension are important. Properties of the lower fluid are denoted by (1) and those of the upper fluid by (2). The two fluids are assumed to be stably stratified by gravity, so $\rho_1 > \rho_2$. The flow is sketched in figure 1. Rectangular coordinates (x, y) are chosen such that the x-axis is horizontal and the y-axis is directed vertically upwards. The interface is located at $y = \eta$ and the origin is chosen so that the mean elevation is zero. A Fourier expansion of the displacement is considered,

$$\eta(x,t) = k^{-1}A_n \mathrm{e}^{\mathrm{i}nk(x-ct)} \quad (n = \pm 1, \pm 2, \ldots). \tag{2.1}$$

Here and subsequently, except as noted, the repeated index implies summation over the complete spectrum. The wavenumber is designated by k and the phase speed by c. The wave amplitude is assumed small enough that only the first few harmonics are important. The relative importance of gravity and surface tension is measured by the dimensionless surface tension κ defined as

$$\kappa = \frac{4\pi^2\sigma}{\rho_1 g L^2}, \tag{2.2}$$

where σ signifies the surface tension.

Miles (1986) has calculated capillary–gravity waves to second order with the hypothesis that $A_n = O(A_1^n)$. He found that progressive waves of permanent form exist for current velocities up to a critical U_c, beyond which the phase velocity c becomes complex. This critical current is given as

$$U_c^2 = U_{c1}^2(1 + \tfrac{1}{2}Ck^2A^2), \tag{2.3}$$

with U_{c1} being the critical current speed calculated from linear theory and A, the wave amplitude, being $A = 2A_1/k$.

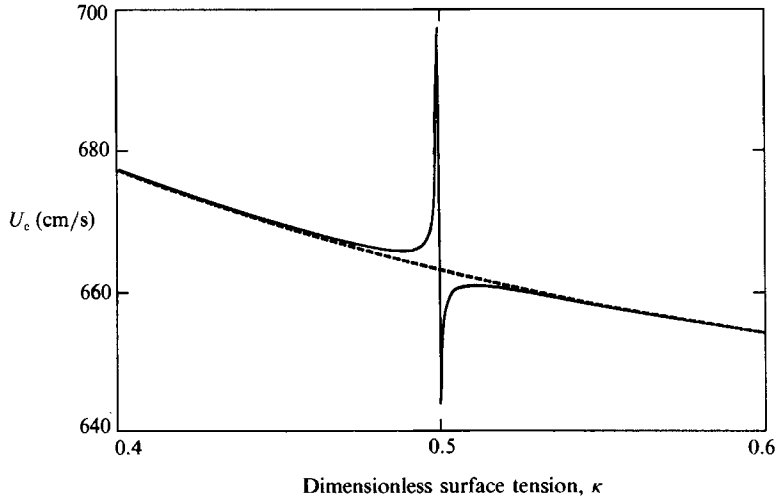

FIGURE 2. The critical current speed U_c as a function of dimensionless surface tension κ, for deep air–water waves. – – –, linear wave; ——, wave with steepness 0.01.

The amplitude of the second harmonic is given by the expression

$$\frac{A_2}{A_1^2} = \frac{1}{2}\left[\frac{2\rho_1 c^2 - 2\rho_2 (U-c)^2}{(\rho_1 - \rho_2) g k^{-1} - 2\sigma k}\right] \equiv B. \tag{2.4}$$

The denominator of B vanishes at the wavenumber k for which the second harmonic of an interfacial gravity–capillary wave of infinitesimal amplitude resonates with the fundamental. It should be noted that the singular wavelength, given by (2.4), depends only on the density ratio (and, in general, the depths) of the two fluids, and not on the current speed. For deep air–water waves ($\sigma = 74$ dynes/cm) this wavelength is 2.44 cm.

The parameter C, defined in (2.3), is important in determining the behaviour in the neighbourhood of the Kelvin–Helmholtz instability. It has been shown that, for pure gravity waves, C at the critical condition is always positive for unbounded fluids (Saffman & Yuen 1982). This implies a stabilization of the interface by the formation of finite amplitude waves. The parameter C has been shown to become negative for all density ratios for thin enough lower films (Bontozoglou & Hanratty 1988) and also for finite-depth fluids in the Boussinesq limit (Miles 1986). For negative C, finite amplitude waves of permanent form cease to exist at current speeds below the linear K–H instability U_{cl}, and for $U > U_{cl}$ no steady-progressive waves of any amplitude exist.

Figure 2 shows the critical current U_c as a function of the dimensionless wavenumber k for a deep air–water wave ($\rho_2/\rho_1 = 0.0013$) with steepness $kA = 0.01$ and wavelength in the vicinity of $L = 2.44$ cm. The dashed line is the critical current speed calculated with linear theory. For a weakly nonlinear wave, the critical air speed is less than for the linear wave when $L < 2.44$ cm ($C < 0$), is greater than for a linear wave when $L > 2.44$ cm ($C > 0$), and is singular at $\kappa = 0.49935$. An inspection of (2.4) indicates that in the neighbourhood of $\kappa = 0.49935$, amplitude A_2 is no longer $O(A_1^2)$ and that the analysis is invalid. It is known that a uniformly valid expansion can be formulated close to the singular point if the ordering $A_2 = O(A_1)$ is adopted (Wilton 1915; Pierson & Fife 1961; Chen & Saffman 1979). Such an expansion is developed in the next section using a Lagrangian formulation.

3. Weakly nonlinear approximation

A horizontally averaged Lagrangian for a two-fluid system with rigid upper and lower boundaries was derived by Miles (1986) to be

$$L = \rho_1 L(q_n, \dot{q}_n, d_1, U_1) + \rho_2 L(q_n, \dot{q}_n, d_2, U_2) - \sigma[\tfrac{1}{2}(\nabla\eta)^2 - \tfrac{1}{8}(\nabla\eta)^4], \tag{3.1}$$

where d_1, d_2 are fluid depths, U_1, U_2 are the ambient horizontal velocities, L is the corresponding Lagrangian of a single layer and q_n is a set of generalized coordinates defined by the Fourier expansion of the interfacial displacement,

$$\eta(x,t) = q_n(t)\,\mathrm{e}^{\mathrm{i}nkx}. \tag{3.2}$$

L may be obtained from the corresponding result for $U = 0$ through the transformation

$$\dot{q}_n(t) = \left(\frac{\mathrm{d}}{\mathrm{d}t} + \mathrm{i}nkU\right) q_n(t) \equiv p_n(t). \tag{3.3}$$

The end result is

$$\begin{aligned} L = \tfrac{1}{2}\rho_{2,1}[&\delta_{nm}\,a_n\,p_m\,p_n \pm \delta_{nm}\,g q_m\,q_n \pm (-\delta_{lnm})(1 + a_m\,a_n\,k_m\,k_n)\,q_l\,p_m\,p_n \\ &+ \delta_{nm}\,a_n\,r_m\,r_n + \tfrac{1}{2}\delta_{jlnm}\{(a_m + a_n)\,k_m\,k_n\,q_j\,q_l\,p_m\,p_n\}]_{2,1}, \end{aligned} \tag{3.4}$$

where

$$\delta_{nm} = \begin{matrix} 1 \\ 0 \end{matrix} \quad \text{for } k_m + k_n \begin{matrix} = 0 \\ \neq 0 \end{matrix}, \qquad \delta_{lnm} = \begin{matrix} 1 \\ 0 \end{matrix} \quad \text{for } k_l + k_m + k_n \begin{matrix} = 0 \\ \neq 0 \end{matrix},$$

and similarly for δ_{jlnm}. Also $r_n = -\delta_{lnm}\,a_m\,k_m\,k_n\,q_l\,p_m$ (n not summed), $a_n = 1/nk$, and $k_n = nk$. The subscripts 2, 1 refer to the upper/lower fluid. Summation with subscripts 2, 1 fixed is implied and the alternative signs in (3.4) correspond to the upper and lower fluids. (For more details see Miles 1986.)

A wave of permanent form is considered so that

$$q_n = k^{-1} A_n\,\mathrm{e}^{-\mathrm{i}nkct} \quad (n = \pm 1, \pm 2, \pm 3, \pm 4), \tag{3.5}$$

where A_n are dimensionless amplitudes. The ordering $A_2 = O(A_1)$, $A_3 = O(A_1^2)$, $A_4 = (A_1^2)$ is postulated. By substituting (3.5) into (3.3) and (3.4), truncating at $n = 4$, which is consistent with a quartic approximation to L, and neglecting terms of order (A_1^5) the following is obtained:

$$\begin{aligned} L = \rho_{2,1} k^{-1}\{&(A_1^2 + 2A_2^2 + 3A_3^2 + 4A_4^2)(U_{2,1} - c)^2 \pm (g/k)(A_1^2 + A_2^2 + A_3^2 + A_4^2) \\ &\pm (U_{2,1} - c)^2(2A_1^2 A_2 + 8A_2^2 A_4 + 8A_1 A_2 A_3) + (U_{2,1} - c)^2(8A_1^2 A_2^2 - A_1^4 - 8A_2^4)\}_{2,1} \\ &- \sigma(A_1^2 + 4A_2^2 + 9A_3^2 + 16A_4^2 - \tfrac{3}{4}A_1^4 - 12A_2^4 - 12A_1^2 A_2^2). \end{aligned} \tag{3.6}$$

To simplify the appearance of the equations, it is postulated that $U_1 = 0$ and $U_2 = U$. This can be done without loss of generality when calculating steady waves. Furthermore, the velocities c and U are non-dimensionalized by dividing by $(g/k)^{0.5}$ and the density ratio $r = \rho_2/\rho_1$ is introduced. As a result the dimensionless number κ, defined by (2.2), appears in the place of surface tension. By requiring $\partial L/\partial A_3 = 0$, $\partial L/\partial A_4 = 0$, the following are obtained:

$$A_5 = 8A_1 A_2 \frac{c^2 - r(U-c)^2}{6[c^2 + r(U-c)^2] - 2(1-r) - 18\kappa}, \tag{3.7}$$

$$A_4 = 8A_2^2 \frac{c^2 - r(U-c)^2}{8[c^2 + r(U-c)^2] - 2(1-r) - 32\kappa}. \tag{3.8}$$

Finally the requirement that $\partial L/\partial A_1 = 0$, $\partial L/\partial A_2 = 0$ gives

$$c^2+r(U-c)^2 = (1-r)+\left(2A_2+4\frac{A_2A_3}{A_1}\right)[c^2-r(U-c)^2]$$
$$-(8A_2^2-2A_1^2)[c^2+r(U-c)^2]+\kappa(1-\tfrac{3}{2}A_1^2-12A_2^2), \quad (3.9)$$

$$2[c^2+r(U-c)^2] = (1-r)+\left(\frac{A_1^2}{A_2}+8A_4+4\frac{A_1A_3}{A_2}\right)[c^2-r(U-c)^2]$$
$$-(8A_1^2-16A_2^2)[c^2+r(U-c)^2]+4\kappa(1-6A_2^2-3A_1^2). \quad (3.10)$$

Either (3.9) or (3.10) can be considered to be the dispersion relation to order $O(A_1^2)$.

4. Influence of current speed on resonance

Equations (3.9) and (3.10) can be combined to derive a relation between the amplitudes A_1 and A_2 that is uniformly valid for all wavelengths. To order A_1^2 the result is

$$A_1^2 = A_2\frac{(1-r)-2\kappa}{2c^2-(1-r)-\kappa}+4A_2^2. \quad (4.1)$$

Equation (4.1) contains the whole phenomenon of gravity–capillary waves in the neighbourhood of the first critical wavelength. For values of κ that are not close to $\frac{1}{2}(1-r)$, $A_2 = O(A_1^2)$ and the Stokes type expansion is recovered. For $\kappa = \frac{1}{2}(1-r)$, equation (4.1) gives $A_1 = \pm 2A_2$ in agreement with Wilton's (1915) result. For $r = 0$ and $U = 0$, (4.1) agrees with the result derived for free-surface waves (Pierson & Fife 1961; Chen & Saffman 1979).

Chen & Saffman (1979) pointed out that (4.1) may be interpreted as specifying A_1 for a given A_2. Then, solutions with $A_1 \neq 0$ exist only if A_2 is such that the right-hand side of (4.1) is positive. Figure 3 shows the accessible regions of the (A_2, κ) plane for $r = 0$, $U = 0$ as the areas outside the two intersecting lines. The inclined line is the locus of (A_2, κ) points (with $A_2 \neq 0$) for which A_1 vanishes. Term A_1 is also zero along the κ-axis. It is important to notice that steady-progressive solutions with $A_1 = 0$, $A_2 \neq 0$ exist everywhere in the neighbourhood of $\kappa = \frac{1}{2}$. These simple waves with two cycles considered as one wavelength (class 2 waves) are not singular close to $\kappa = \frac{1}{2}$. Chen & Saffman (1979) demonstrated that for $\kappa \neq \frac{1}{2}$ a bifurcation can occur for which the wavelength of this simple wave doubles ($2 \to 1$ bifurcation). Consider, for example, a class 2 wave with $\kappa > \frac{1}{2}$, $A_2 > 0$ that is growing in amplitude (the dashed line in figure 3). Such a wave is unique until A_2 reaches a critical value (where the dashed line intersects the $A_1 = 0$ curve). Here the pure wave can (but, need not) bifurcate by adding a $A_1 \neq 0$ subharmonic and, therefore, double its wavelength. The situation is similar for $\kappa < \frac{1}{2}$ and $A_2 < 0$.

Figure 4 demonstrates the change in the accessible region on the (A_2, κ)-plane for air–water waves ($r = 0.0013$) moving in the direction of the wind. The lines are the loci of the points for which $A_1 = 0$ is calculated with (4.1) for different air velocities. The accessible regions are contained in the oblique angles defined by the inclined line and the κ-axis. It is evident that, as the air velocity increases, the bifurcation loci become more inclined and approach the horizontal. The change is insignificant for small air velocities but becomes important close to conditions required for a K–H instability. Consider, for example, a pure class 2 wave that is growing in amplitude. Figure 4 indicates that, as the air velocity increases, the wave needs to reach a higher

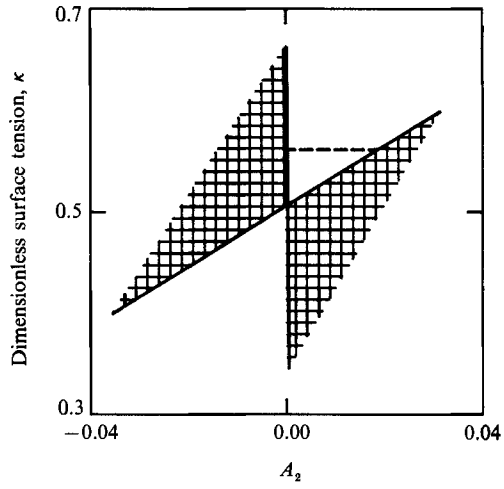

FIGURE 3. The accessible region of the (A_2, κ)-plane for free-surface waves (shaded areas).

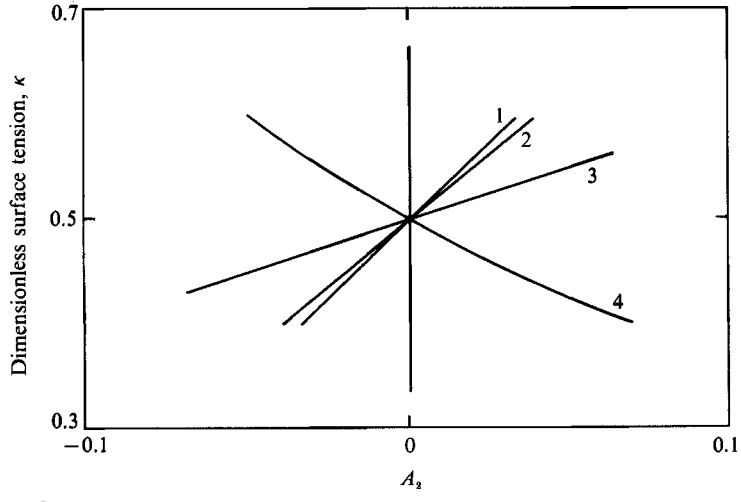

FIGURE 4. The accessible region of the (A_2, κ)-plane for air–water waves and different current velocities U. 1: $U = 0$; 2: $U = 200$ cm/s; 3: $U = 400$ cm/s; 4: $U = 600$ cm/s.

amplitude before it is able to bifurcate. For even higher air velocities the loci for bifurcation have a negative inclination to the horizontal, whose value increases monotonically with increasing velocity. Solutions with $A_1 \neq 0$ exist within the region outlined by the oblique curves; therefore, the bifurcation for $\kappa > \frac{1}{2}(1-r)$ will now be associated with $A_2 < 0$.

There is a range of air velocities for which the bifurcation loci are very close to the horizontal. This implies that, unless κ has a value very near to the critical, the $2 \to 1$ bifurcation will not happen. An inspection of (4.1) indicates that this phenomenon is associated with the denominator of the first term on the right-hand side becoming very small. Indeed, by using the linear dispersion relation and considering the physically important case of waves moving in the same direction as the wind, one can compute the singular air velocity to be

$$U_s = \left(1 + \frac{1}{r^{\frac{1}{2}}}\right)(\tfrac{1}{2}[(1-r)+\kappa])^{\frac{1}{2}}. \tag{4.2}$$

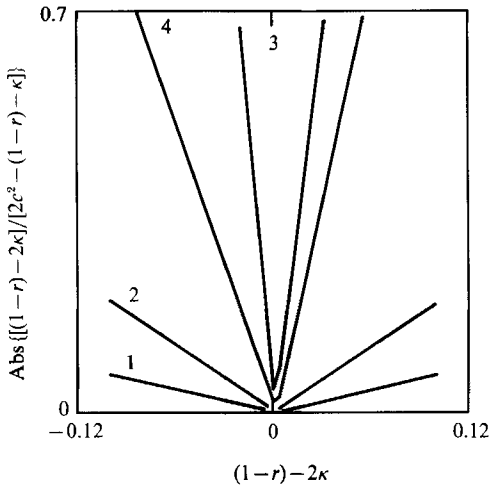

FIGURE 5. Coefficient of the order $O(A_2)$ term in (4.1) *vs.* κ, for different current velocities U. 1: $U = 0$; 2: $U = 400$ cm/s; 3: $U = 480$ cm/s; 4: $U = 500$ cm/s.

For this air velocity the denominator in (4.1) is, to first order, equal to zero. It is interesting to compare U_s with the critical K–H current velocity beyond which linear steady waves cease to exist. This is found from the linearized form of (3.9) to be

$$U_{cl}^2 = \frac{1+r}{r}[(1-r)+\kappa]. \tag{4.3}$$

It is observed that the singular current velocity U_s is always smaller than U_{cl}, and approaches U_{cl} as $r \to 1$.

For current velocities close to U_s, there is a profound change in the importance of the resonance interaction. Note from (4.1) that the amplitudes of the second and first harmonics are comparable when the coefficient of the A_2-term becomes very small (of order $O(A_2)$). This coefficient is plotted versus $(1-r)-2\kappa$ in figure 5 at different air velocities for waves at the interface between air and water. The important conclusion is that, for air velocities close to U_s the magnitude of this coefficient is large everywhere except in a very narrow band around the resonant wavelength. Therefore, the resonant interaction is significant only extremely close to $\kappa = \frac{1}{2}(1-r)$ and the Stokes-type expansion with $A_2 = O(A_1^2)$ is valid everywhere else.

5. Numerical method

Velocity potentials ϕ_1, ϕ_2 and stream functions ψ_1, ψ_2 independent of time are defined for the two fluids. The physical coordinates are expressed as Fourier series of ϕ_1, ψ_1 below the interface and of ϕ_2, ψ_2 above the interface in the following way:

$$\left.\begin{aligned} x_1 &= \frac{\phi_1}{c} + \sum_1^N a_{1,n} \sin\left(\frac{\phi_1}{c}\right) e^{n\psi_1/c}, \\ y_1 &= \frac{\psi_1}{c} + a_{1,0} + \sum_1^N a_{1,n} \cos\left(n\frac{\phi_1}{c}\right) e^{n\psi_1/c}, \end{aligned}\right\} \tag{5.1}$$

$$\left.\begin{aligned} x_2 &= \frac{\phi_2}{c} + \sum_1^N a_{2,n} \sin\left(n\frac{\phi_2}{c}\right) e^{-n\psi_2/c}, \\ y_2 &= \frac{\psi_2}{c} + a_{2,0} - \sum_1^N a_{2,n} \cos\left(n\frac{\phi_2}{c}\right) e^{-n\psi_2/c}. \end{aligned}\right\} \tag{5.2}$$

On the interface, which is chosen to be $\psi_1 = \psi_2 = 0$, the tangential velocities below and above are given by

$$q_1 = -c\left\{\left[1 + \sum_1^N n a_{1,n} \cos\left(n\frac{\phi_1}{c}\right)\right]^2 + \left[\sum_1^N n a_{1,n} \sin\left(n\frac{\phi_1}{c}\right)\right]^2\right\}^{\frac{1}{2}}, \tag{5.3}$$

$$q_2 = (U-c)\left\{\left[1 + \sum_1^N n a_{2,n} \cos\left(n\frac{\phi_2}{c}\right)\right]^2 + \left[\sum_1^N n a_{2,n} \sin\left(n\frac{\phi_2}{c}\right)\right]^2\right\}^{\frac{1}{2}}. \tag{5.4}$$

The inequality of the velocity potentials of the two fluids at the interface is reconciled by defining the variables

$$s = 0.5[(\phi_2/c) - (\phi_1/c)], \tag{5.5}$$

and

$$\xi = (\phi_2/c) - s = (\phi_1/c) + s, \tag{5.6}$$

where ϕ_1, ϕ_2 are the values of the velocity potentials on the interface. The equations are discretized by $N+1$ points from the crest to the trough as follows:

$$\xi_i = (i-1)\pi/N \quad (i = 1, 2, \ldots, N+1). \tag{5.7}$$

The Bernoulli equation

$$\tfrac{1}{2}q_1^2 - \tfrac{1}{2}rq_2^2 + (1-r)\eta - \kappa R^{-1} = b, \tag{5.8}$$

provides one set of $N+1$ equations, to be satisfied at each ξ_i. In (5.8) lengths are normalized with the inverse wavenumber $k^{-1} = L/2\pi$ and velocities, with $(g/k)^{\frac{1}{2}}$. Term r is the ratio of densities and κ is a dimensionless surface tension defined by (2.2). Term R is the radius of curvature and its inverse equals

$$R^{-1} = \frac{\mathrm{d}^2\eta/\mathrm{d}x^2}{[1 + (\mathrm{d}\eta/\mathrm{d}x)^2]^{\frac{3}{2}}} = \frac{x'y'' - x''y'}{(x'^2 + y'^2)^{\frac{3}{2}}}, \tag{5.9}$$

where x', y', etc. are derivatives with respect to ξ of the interface coordinates x, y.

The requirement that $x_1 = x_2$ and $y_1 = y_2$ at each one of the $N+1$ points along the interface produces the following equations:

$$\xi - s + \sum_1^N a_{1,n} \sin[n(\xi - s)] = \xi + s + \sum_1^N a_{2,n} \sin[n(\xi + s)], \tag{5.10}$$

$$a_{1,0} + \sum_1^N a_{1,n} \cos[n(\xi - s)] = a_{2,0} - \sum_1^N a_{2,n} \cos[n(\xi + s)]. \tag{5.11}$$

The auxiliary equations for the crest and trough

$$s(0) = s(\pi) = 0, \tag{5.12}$$

satisfy (5.10) identically at the end points and leave the values of s at the other $N-1$ points as unknowns. The value of $a_{1,0}$ affects only the mean interfacial elevation. It is taken as $a_{1,0} = 0$. The mean elevation $\bar{y}$ is calculated and then $a_{1,0} = -\bar{y}$, $a_{2,0} = a_{2,0} - \bar{y}$, $b = b + (1-r)\bar{y}$. This leaves the $3N+2$ unknowns, $a_{1,1}, \ldots, a_{1,N}, a_{2,1}, \ldots, a_{2,N}$,

$s_2, \ldots, s_N$, $a_{2,0}$, c, b to be defined by the $3N+1$ equations (5.8), (5.10) and (5.11). A definition of the wave magnitude (either the wave height or the amplitude of the main harmonic) provides the last equation.

The system is solved by Newton's method. Accuracy is tested by the independence of the results on the value of N. The magnitude of error is monitored by the ratio of the last to the first Fourier coefficient. (For more details, see Saffman & Yuen 1982). The method works extremely well for waves of small to moderate amplitude. However, beyond some steepness the accuracy decreases rapidly and cannot be recovered by reasonable increases in N (values up to $N = 100$ were used). Chen & Saffman (1980) used a hodograph-plane Fourier method for free-surface waves and had no difficulty reaching waves of maximum height. Such waves were always limited by the profile enclosing one or more bubbles, so that a further increase in height would result in the surface crossing itself. It is evident that such a configuration leads to profile singularities for only the upper fluid (a cusp at the contact point). Therefore, the failure of the present work to obtain the highest waves is not surprising. It should be noted that an integro-differential analysis of interfacial waves (Vanden-Broeck 1980) also failed to reach the limiting profile but there was evidence that the limit wave would exhibit trapped bubbles.

6. The finite-amplitude $2 \rightarrow 1$ bifurcation

The numerical method described in §5 was used to calculate the bifurcation curve discussed in §4 for waves of finite amplitude. A range of dimensionless surface tensions of $\frac{1}{2} \geqslant \kappa \geqslant \frac{1}{6}$ was examined. For air–water waves this corresponds to wavelengths (before the $2 \rightarrow 1$ bifurcation) of $1.22 \text{ cm} \leqslant L \leqslant 2.11 \text{ cm}$. Since the ripples first observed in gas–liquid flows are 1.5–2.0 cm in length, the above range was adequate for the purposes of this paper. Starting with $\kappa = \frac{1}{2}$ for a small amplitude wave of class 2, the amplitude was increased until a change of sign of the determinant of the Jacobian matrix occurred. This indicated that the solution branch went through a critical point. Since all variables were changing monotonically, a crossing of the bifurcation curve had taken place. The calculation was repeated for a number of values of $\kappa < \frac{1}{2}$ and for different current velocities U to investigate the effect of wind speed on the bifurcation of finite-amplitude waves. Since the wavelength is changing with changing κ, the dimensionless current velocity $U/(g/k)^{\frac{1}{2}}$ varies as well. It was, therefore, decided it would be more useful to find the bifurcation locus for a constant dimensional velocity. The sign-change method for determining the bifurcation locus worked extremely well for small-to-moderate current velocities, and the accuracy was again tested by the independence of the results on the value of N ($N = 20$, 40, 60 were used). However, for high current velocities, the Jacobian started changing sign irregularly beyond some wave height, and the results were dependent on the value of N. Increasing N produced more irregular results, even though the wave properties, calculated for all values of N, were exactly the same. The reason for this irregular behaviour is not known.

Figure 6 shows the amplitude of a class 2 air–water wave at which bifurcation occurs, for current velocities 0, 2.0, 2.5, 3.5, 4.0 and 6.0 m/s. The uncertainties in the values of κ and $a_{1,2}$ are 0.002 and 0.001 respectively. (The term $a_{1,2}$ is the steepness normalized with the wavelength after bifurcation and, therefore, is related to the steepness of the small ripples by $kA = 2a_{1,2}$.) As noted by Chen & Saffman (1980), many Fourier components are introduced when bifurcation occurs at finite amplitude. Thus, the return of the bifurcation locus to the κ-axis is the result of the

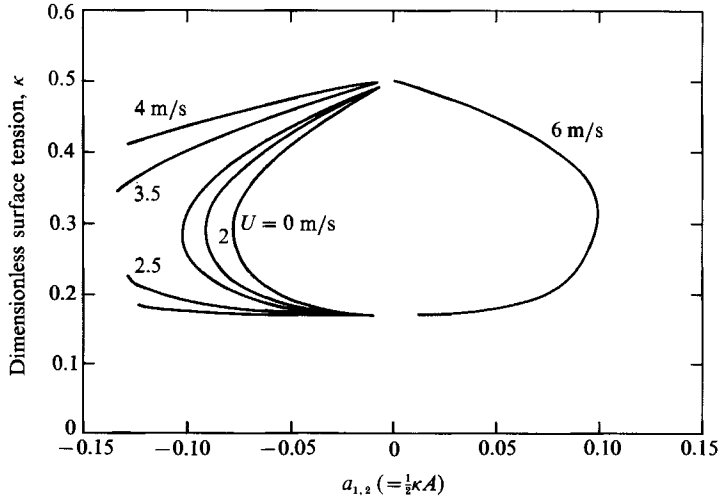

FIGURE 6. The amplitude of a class 2 air–water wave at which bifurcation occurs, for current velocities 0, 2.0, 2.5, 3.5, 4.0 and 6.0 m/s.

$a_{1,3}$ harmonic becoming increasingly more important with decreasing κ. For $\kappa \approx \frac{1}{6}$ the locus actually represents a $2 \rightarrow 3$ bifurcation.

For zero current velocity the bifurcation curve agrees with the one calculated by Chen & Saffman (1980) for free-surface waves. Increasing the current velocity postpones the bifurcation to higher waves for all wavelengths considered. However, as current velocity approaches the critical condition for a K–H instability the wave height at which bifurcation occurs decreases again, as shown by the locus for $U = 6$ m/s in figure 6. For $\kappa \approx \frac{1}{2}$ the numerical results agree with the prediction of the weakly nonlinear theory of §4.

Choi (1977) observed experimentally a doubling of wavelength for capillary–gravity waves produced by wind blowing at 5 m/s over water. The waves that were generated first had a wavelength of 1.8 cm. As they propagated downstream they grew in amplitude and, eventually, doubled in wavelength at a certain fetch. The wave height at which the dominant frequency changed was roughly estimated by Chen & Saffman (1980) to be 1.7 mm. (In the present notation this is equivalent to $a_{1,2} = 0.15$.) (Note that A_2 in Chen & Saffman's definition of the Fourier series is twice as large as $a_{1,2}$ in the present work.) The value of κ corresponding to the above experiment was 0.23 ($\sigma = 74$ dynes/cm) and figure 6 indicates that bifurcation for $\kappa = 0.23$ and $a_{1,2} = 0.15$ roughly occurs for a wind velocity of 4.0–4.5 m/s. Although the agreement is not exact it indicates that the effect of wind is probably correctly taken into account.

7. Kelvin–Helmholtz instability

It can be seen from the dispersion relation (equation (3.9)) that for linear waves, and given values of density ratio r and current velocity U, there are two solutions corresponding to the two roots of the quadratic equation for c. Such steady solutions cease to exist when U exceeds a critical value U_{cl} given by

$$U_{\mathrm{cl}}^2 = \frac{1+r}{r}[(1-r)+\kappa], \tag{7.1}$$

with $$c_{c1}^2 = \frac{r[(1-r)+\kappa]}{1+r}. \tag{7.2}$$

For finite amplitude waves, (3.9) gives the dispersion relation valid to order A_1^2. Its form indicates that the critical current, U_c, beyond which steady solutions no longer exist is a function of the wave magnitude. To derive an equation valid in the neighbourhood of the K–H instability the expression for A_3 (equation (3.7)) is substituted into (3.9) and the phase speed at the critical point, calculated from the lower-order dispersion relation, is backsubstituted in (3.9). It should be noted that the dispersion relation is used up to order $O(1)$ in some terms of (3.9) and up to order $O(A_1)$ in others to keep the entire expression valid to $O(A_1^2)$. The end result is the following equation:

$$c^2+r(U-c)^2 = [(1-r)+\kappa]\left\{1-\frac{\kappa}{(1-r)+\kappa}(\tfrac{3}{2}A_1^2+12A_2^2)\left(\frac{1-r}{1+r}\right)\right.$$
$$\left.+4A_2^2\left(\frac{1-r}{1+r}\right)^2\frac{3(1-r)-\kappa}{(1-r)-3\kappa}+(2A_1^2-8A_2^2)\right\}. \tag{7.3}$$

Equation (7.3) is uniformly valid for wavelengths close to the resonance condition. It will be used in combination with (4.1), which supplies the relation between the amplitudes of the first two harmonics. For wavelengths such that κ is not close to $\frac{1}{2}(1-r)$, equation (4.1) gives A_2 of order $O(A_1^2)$; and substitution into (7.3) recovers the results of Miles (1986) and Nayfeh & Saric (1972).

To describe the results for wavelengths close to the resonance, a measure of the wave magnitude needs to be defined. When $A_1 \gg A_2$ the crest-to-trough distance is used to characterize the wave since it is a monotonic function of the wave size. When both harmonics are significant such a measure could be misleading. Instead it is proposed to use the 'combined' wave steepness given by

$$\epsilon = 2(A_1^2+4A_2^2)^{\frac{1}{2}}. \tag{7.4}$$

For $A_1 \gg A_2$, $\epsilon = 2A_1 = kA$ in agreement with the conventional definition of wave steepness. For $A_1 \ll A_2$, $\epsilon = 2(2A_2)$ and, since the physically significant wavelength (associated with A_2) is half of the nominal, ϵ equals the actual wave steepness. This expression can be generalized and used to describe higher-order resonances as well as the highly nonlinear resonant waves that are generated numerically.

Air–water waves are considered first, by choosing a density ratio $r = 0.0013$. The relative magnitude of the amplitudes A_1, A_2 at the K–H instability is derived from (4.1) by substituting the critical linear phase speed from (7.2). The results for a wave with steepness $\epsilon = 0.01$ are shown in figure 7. It is evident that close to $\kappa = 0.49935$ there are two wave families, each of which eventually degenerates to a pure wave with half the original wavelength ($A_1 = 0$). The critical current velocity beyond which steady solutions cease to exist is shown as a function of κ in figure 8 for $\epsilon = 0.01$. A comparison with figure 2 indicates that the singularity has been removed. The dashed curve represents the critical current, U_c, for a pure class 2 wave ($A_1 = 0, A_2 \neq 0$) with $\epsilon = 0.01$. The two solution families meet this curve when $A_1 = 0$, as expected from the above observations.

A steady wavetrain under the action of wind is more conveniently viewed as having a constant wavelength (at least for a short time) and as growing in amplitude. Therefore, it is of interest to investigate the dependence of the critical current speed U_c on the wave steepness ϵ. Equations (7.3) and (4.1), together with the definition of the wave steepness, are used and the results for selected values of κ are shown in

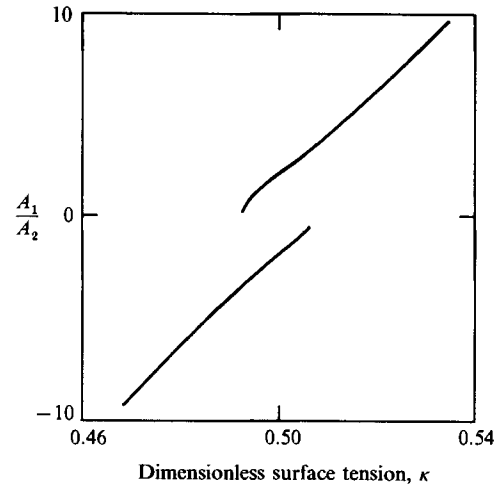

FIGURE 7. Relative magnitude of the first two harmonics for an air–water wave with steepness $\epsilon = 0.01$.

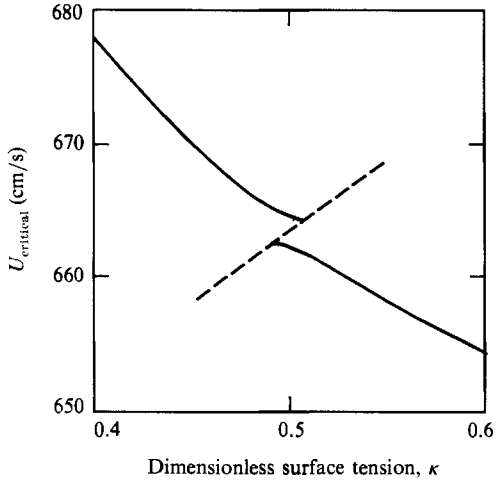

FIGURE 8. Critical current velocity U_c for an air–water wave with steepness $\epsilon = 0.01$. ---, uniformly valid expansion; ---, U_c for pure class 2 wave.

figure 9. For $\kappa = 1.0$, $(U_c^2/U_{c1}^2)-1$ is proportional to ϵ^2 in agreement with (2.3) and the K–H instability is subcritical for finite amplitude waves. The same functionality holds for $\kappa = 0.1$, only now with a positive slope. For κ larger than 0.499 35 and approaching it, the K–H instability becomes increasingly subcritical up to $\kappa =$ 0.499 35. Very close to the resonance there also exists a second solution which shows a more complicated behaviour: The critical current initially increases with steepness, reaches a maximum and decreases again. As a result, progressive waves of permanent form exist only up to current velocities a little higher than the critical linear U_{c1}. For a supercritical current velocity in this range the steepness of steady waves has both a maximum and a minimum allowable value. A similar behaviour is depicted for $\kappa = 0.45$. For longer waves, resonances of higher order are expected to become important (Chen & Saffman 1979). However, this was not pursued in the present work.

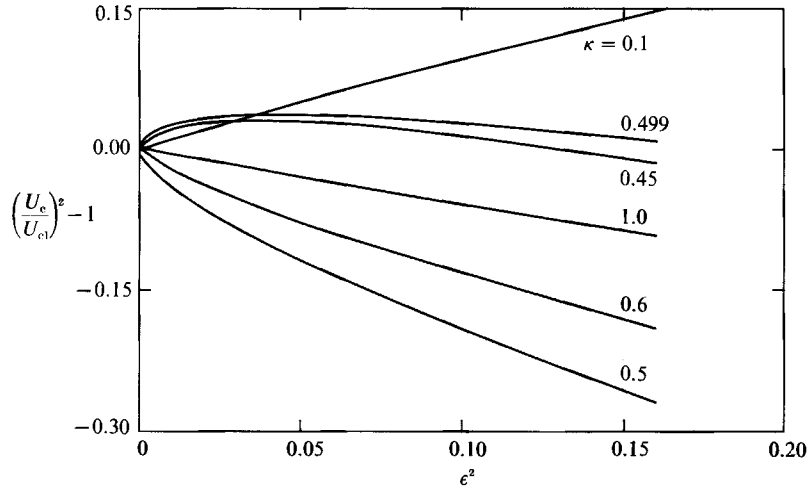

FIGURE 9. The critical current velocity U_c as a function of the wave steepness ϵ to second order, for various wavelengths.

The present results indicate that, for wavelengths smaller than the resonant and approaching it, the K–H instability becomes increasingly subcritical. Therefore, for a given current velocity, smaller than U_{cl}, steady progressive waves can only grow up to a maximum steepness. However, they can further evolve by a $2 \rightarrow 1$ bifurcation, if they have reached the height that allows the bifurcation to take place. It is, therefore, possible that the two phenomena studied in the present work are related in that the K–H instability could be triggering the occurrence of the $2 \rightarrow 1$ bifurcation.

The ripples that are first observed in gas–liquid flows have wavelengths of 1.5 to 2.0 cm, so the $2 \rightarrow 1$ bifurcation takes place at finite amplitude. Such wavelengths are far enough from the resonant wavelength of 2.44 cm that the weakly nonlinear results for a K–H instability, based on the ordering $a_{1,2} = O(a_{1,1}^2)$ (Miles 1986), are valid. Numerical calculations for waves with lengths 1.5–2.0 cm indicate that there are only small deviations from the weakly nonlinear results for steepness kA up to 0.35 ($a_{1,60}/a_{1,1} \approx 10^{-5}$ for $N = 60$).

The main conclusion from the weakly nonlinear analysis (Weissman 1979; Miles 1986) is that, for the wavelengths presently considered, the K–H instability is subcritical and described by the equation

$$U_c^2 = U_{cl}^2(1 + Ck^2A^2), \tag{7.5}$$

where C is a parameter, depending on the wavelength and density ratio, which is negative for air–water waves with wavelengths less than 2.44 cm. Furthermore, Miles (1986, his equation (4.12)) showed that such waves become unstable for

$$k^2A^2 > \tfrac{2}{3}(k^2A^2)_{\max}. \tag{7.6}$$

The above results are depicted in figure 10(a, b) for ripples with wavelengths (before bifurcation) of $L = 1.6$ cm (a) and $L = 1.93$ cm (b). Curve (1) is the K–H limit to the existence of progressive waves of permanent form and curve (2) is the steepness at which such waves become unstable, as given by (7.6). It is noted that both of these curves give the linear critical current velocity, U_{cl}, for a wave of zero height and a decreasing critical current velocity with increasing wave steepness. The

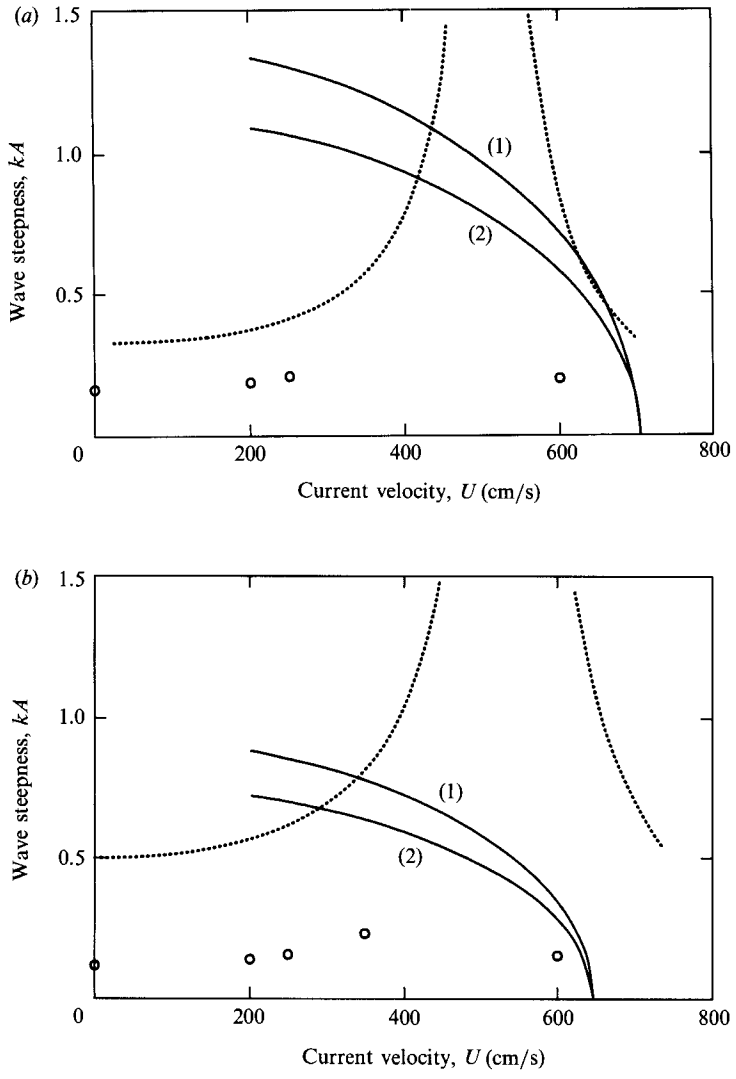

FIGURE 10. Dependence of the wave steepness on the current velocity U for: ——(1), the K–H limit to the existence of steady waves; ——(2), the stability limit of steady waves; ○, the finite-amplitude bifurcation; ..., the weakly nonlinear bifurcation. (*a*) Ripples with L (before bifurcation) 1.6 cm. (*b*) $L = 1.93$ cm.

dotted curve is the height at which the $2 \rightarrow 1$ bifurcation can take place according to the weakly nonlinear theory; the circles are the heights calculated by the numerical method described in §5. As expected, the weakly nonlinear results become increasingly inaccurate away from $L = 1.22$ cm. (Note that $a_{1,2}$ of figure 6 is normalized with the wavelength after bifurcation and, therefore, is related to the steepness of the wave kA by $kA = 2a_{1,2}$.) These dotted curves approach asymptotically the singular current velocity (equation (4.2)), so that an arbitrarily large wave steepness is required close to U_s. A rough extrapolation of the bifurcation curve, based on a knowledge of the behaviour close to U_s obtained from the weakly nonlinear results (see §4), indicates that it meets the instability curve (2) at a current velocity $U_b \approx 4.5$ m/s. For $U < U_b$ the bifurcation loci are below curve (2), so a

steady wave can grow in height without changing wavelength. It can, therefore, be speculated that the bifurcation is taking place for $U \geqslant U_b$.

The value of the critical current velocity (being close to U_s) is not very sensitive to the initial wavelength in the range 1.5–2.0 cm. What mainly varies is the wave steepness at which the bifurcation occurs. For example, calculations for the length $L = 1.93$ cm, presented in figure 10(*b*), suggest that bifurcation occurs at smaller steepness than for $L = 1.6$ cm.

The above results are strictly valid for deep fluids. For the range of wavelengths considered, they are applicable to gas and liquid streams with thickness $h_{G,L} \geqslant 1$ cm. The main conclusion from the analysis is that, if small ripples exist at the gas–liquid interface, they can bifurcate at current velocities above a limiting value. This transition velocity, which is smaller than U_{cl}, should be insensitive to changes in the gas and liquid thicknesses $h_{G,L}$, as long as $h_{G,L} \geqslant 1$ cm. This last condition, that the actual current velocity is independent of the gas space thickness, is crucial for the discussions presented in the next section.

8. Transition to slug flow

The transition from a stratified pattern to a slug pattern for horizontal gas–liquid flow has been the subject of a number of theoretical studies. Kordyban & Ranov (1970), Wallis & Dobson (1973) and Taitel & Dukler (1976), among others, considered a K–H instability mechanism for long wavelength disturbances and incorporated semi-empirical corrections for nonlinear effects. Lin & Hanratty (1986) included viscous effects in a linear analysis of long wavelength disturbances. They were able to show that viscosity is destabilizing for long wavelength disturbances on low-viscosity liquids; this provided an explanation for the occurrence of the transition at current velocities below the inviscid K–H prediction. However, Andritsos *et al.* (1989), working in a 4-inch pipeline with air and water–glycerine solutions with viscosities 1, 20 and 100 cP, showed that the analysis of Lin & Hanratty does not correctly predict the onset of slug flow for very viscous liquids. Furthermore, they observed that the precursor to the creation of a slug is the formation of small ripples which suddenly evolve into a long wave. If the gas space is small enough, such a wave grows to cover the entire cross-section and, therefore, creates a slug. This observation was facilitated because the interface is smooth up to the transition point for very viscous liquids ($\mu \geqslant 20$ cP). This is not the case for the air–water interface, which is covered by ripples generated at much lower gas velocities by a mechanism that considers energy supplied to the waves by pressure variations in phase with the wave slope (Miles 1957; Hanratty 1983).

The observations of Andritsos *et al.* (1989) and their data are used in the present work in conjunction with the theory developed in §§6 and 7. The $2 \rightarrow 1$ bifurcation, discussed earlier, is postulated to be the first step in the process leading from ripples to large disturbances, and eventually to slugs. A crucial test is to demonstrate that the transition velocity is independent of the fluid depth, since the current velocity should be proportional to the square root of the gas space thickness (Wallis & Dobson 1973) if the slugs originate from infinitesimal long waves.

Two cases are distinguished: for very viscous liquids ($\mu = 20$–100 cP) there are no ripples on the interface at small current velocities, since such ripples are created on viscous liquids by a K–H mechanism (Miles 1959). Therefore, the transition to slugs is expected to occur as soon as the ripples appear, at the critical K–H current velocity. For water (and other low-viscosity fluids) such ripples are created at gas

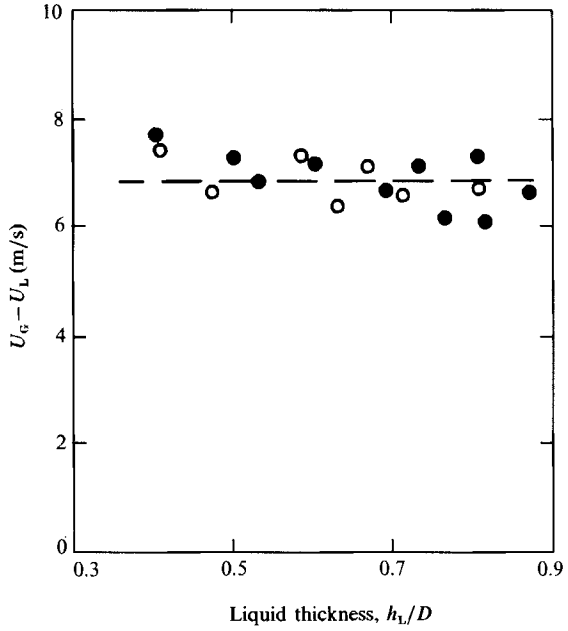

FIGURE 11. The current velocity U at transition to slugs as a function of the liquid film thickness, for viscous liquids (Data from Andritsos *et al.* 1989). Viscosity = 20–100 cP; ●, $D = 9.53$ cm; ○, $D = 2.52$ cm.

velocities below that needed for a K–H instability (≈ 1 m/s, Miles 1957). Therefore, the arguments of §7 are applicable and slugs are expected to form at a constant velocity, if they originate from these small ripples.

The data taken by Andritsos *et al.* are used in figures 11 and 12. The gas and liquid volumetric flow rates are converted to actual velocities by using the measured liquid thickness and a plug flow assumption. Figure 11 shows the results for the viscous liquids. The transition to slugs occurs at a relative current velocity of 6.5–7.0 m/s, in agreement with the linear K–H instability prediction, for both 1-inch and 4-inch pipes. Furthermore, changing the viscosity from 20 to 100 cP has no effect on the transition, which supports the inviscid theory explored in this paper.

The theory developed in §7 indicates that the bifurcation height decreases as the current velocity approaches the critical for a linear K–H instability. For higher current velocities steady wave solutions do not exist because the K–H instability is subcritical for wavelengths $L < 2.44$ cm. More information can, however, be extracted from the theory if the critical phase speed c_{cl} at the K–H instability

$$c_{cl} = \frac{rU}{1+r} \tag{8.1}$$

is used in (4.1) to calculate the bifurcation steepness,

$$kA = \frac{1}{2}\frac{(1+r)^2}{1-r}\frac{(1-r)-2\kappa}{rU^2}. \tag{8.2}$$

Equation (8.2) shows that the height for the $2 \to 1$ bifurcation to take place varies as U^{-2} in the neighbourhood of the K–H instability. Therefore, it becomes very small for high current velocities. This is in agreement with the observations on viscous

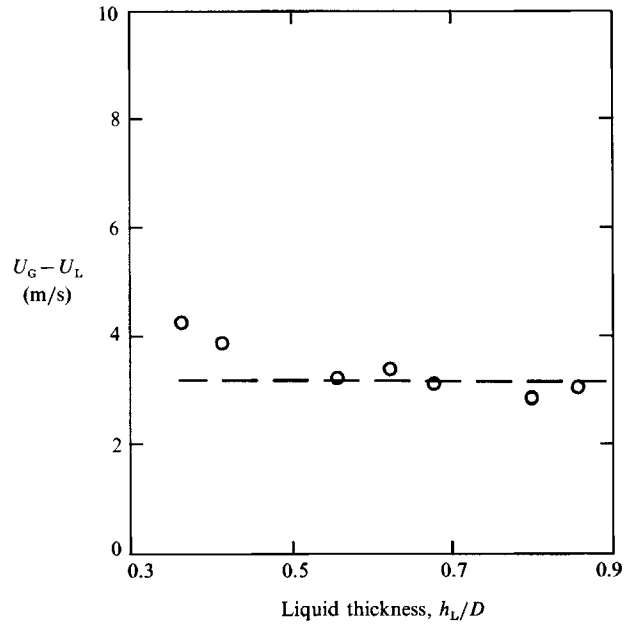

FIGURE 12. The current velocity U at transition to slugs as a function of the liquid film thickness for water (Data from Andritsos *et al.* 1989). Viscosity = 1 cP; D = 9.53 cm.

fluids that the ripples evolve to long waves very fast and that slugs form close to the entrance.

The results for air–water are shown in figure 12. When there is a hydraulic gradient along the pipe (small gas velocities) the value of the liquid thickness used is the one close to the inlet. This can be justified by arguing that the highest liquid thickness corresponds to the most unstable condition. However, it is contradictory to the theoretical prediction and laboratory observations that the ripples need to reach a finite amplitude to bifurcate and, therefore, that the slugs should form downstream. Figure 12 shows that, with the use of the inlet liquid thickness, the transition current velocity remains constant at around 3.0–3.5 m/s. This, however, is much lower than the 4.5 m/s that was theoretically estimated in §7. If the average liquid thickness is used instead of the inlet value, the transition current velocity does not even remain constant.

Experiments with smaller pipe diameters have shown that in a range of diameters of 2.52–9.53 cm there is a definite effect of pipe diameter on the initiation of slugs in air–water flows. This is not predicted by the present theory but is successfully modelled by assuming that the slugs originate from the growth of small-amplitude long waves (Lin & Hanratty 1986). The long wavelength theory provides an instability mechanism at lower current velocities than the present theory and, as a result, is the important one for air–water in small pipes. For large diameter pipes, the long wavelength theory predicts unrealistically high current velocities, so it is plausible to assume slugs appear as a result of nonlinear growth of small ripples. This, however, needs to be investigated.

9. Concluding remarks

This paper examines the effect of current velocity on capillary–gravity waves at wavelengths close to where resonance has been observed for free waves.

The wavelengths over which resonant (or near-resonant) interactions occur is found to be affected strongly by current velocity. This range decreases with increasing gas velocity until at a singular gas velocity, U_s, defined by (4.2), it occurs in an arbitrarily small range of wavelengths. For still higher gas velocities the range increases. This singular velocity is always smaller than the critical current velocity, U_{cl}, beyond which linear steady waves cease to exist.

Chen & Saffman have shown that when free surface waves in the capillary–gravity range reach a certain height a bifurcation is possible whereby a doubling of the wavelength occurs. It is shown that the presence of a current velocity increases the height required for this bifurcation. This effect of current velocity is particularly strong in the neighbourhood of U_s. However, as the current velocity approaches U_{cl} the height required for bifurcation decreases again.

Previous studies have shown that the nonlinear Kelvin–Helmholtz instability is subcritical at wavelengths smaller than the resonant wavelength. That is, the critical current velocity at which finite amplitude waves cease to exist decreases with increasing amplitude. However, these analyses are not valid in the neighbourhood of the resonant wavelength. The present analysis extends this previous work by resolving the characteristics of the K–H instability of finite amplitude waves close to resonance. An interesting new result that evolves is that for waves with wavelengths shorter than the resonant wavelength and approaching it (capillary-side waves) the K–H instability becomes increasing subcritical.

The prediction of the possibility of a bifurcation does not mean that one will occur. A consideration of the few experimental results which seem to be manifesting this phenomenon has led us to postulate that a K–H instability can trigger a bifurcation.

A number of studies have been carried out in which wave development with increasing fetch has been examined for air–water flow. The first ripples are regular and have a wavelength of 1.5–2.0 cm. They appear to be generated by a sheltering mechanism whereby energy is fed to the waves by wave-induced pressure variations in the gas flow that are in phase with the wave slope (Cohen & Hanratty 1965). With increasing fetch the complexity of the waves and the dominant wavelength increases. A number of investigators have obtained results that suggest that the first step in this process of wave development is a bifurcation. The argument that this bifurcation is triggered by a subcritical K–H instability gives the result that the bifurcation will occur for the air–water system at current velocities greater than 4.0–4.5 m/s for wavelengths in the range 1.5–2.0 cm. This prediction, as well as the prediction of the height at which bifurcation will occur, are consistent with experimental observations.

Furthermore, the postulate that a K–H instability can trigger a bifurcation provides an interpretation of recent studies of the initiation of slugs for gas–liquid flow in a pipeline by Andritsos *et al.* (1989). They found for viscous liquids (greater than 20 cP) that slugs evolve from short capillary–gravity waves generated by a K–H instability. The present analysis shows that a bifurcation is possible when these waves grow just slightly in height. It is, therefore, proposed that this bifurcation is the first step in the evolution of these ripples to a slug.

Bifurcation is not possible on these viscous liquids at lower gas velocities than U_{cl} since no waves exist. However, for air–water flows capillary–gravity waves generated by a sheltering mechanism exist at current velocities less than U_{cl}. It is possible for

these to grow to a height where a bifurcation is triggered by a subcritical K–H instability. On the basis of these observations it is predicted that slugs can be generated at a gas velocity of 4.5 m/s for air–water flows.

Observations in pipelines with diameters of 9.53 cm and less are contrary to this result in that slugs are generated at lower gas velocities and in that there is an effect of the height of the gas space. It appears that the direct growth from a long wavelength disturbance (Lin & Hanratty 1986) is the correct explanation of these results. However, it is possible that an evolution from small wavelength waves causes slugging for air–water flow in large diameter pipes and that the estimated critical velocity of 4.5 m/s is applicable.

This work is supported by the National Science Foundation under Grant 88-00980 and by the Department of Energy under Grant DEF G02-86ER13556.

REFERENCES

ANDRITSOS, N., WILLIAMS, L. & HANRATTY, T. J. 1989 Effect of liquid viscosity on stratified-slug transition in horizontal pipe flow. *Intl J. Multiphase Flow* **15**, 877.

BONTOZOGLOU, V. & HANRATTY, T. J. 1988 Effects of finite depth and current velocity on large amplitude Kelvin–Helmholtz waves. *J. Fluid Mech.* **196**, 187.

CHEN, B. & SAFFMAN, P. G. 1979 Steady gravity–capillary waves on deep water. I. Weakly nonlinear waves. *Stud. Appl. Maths* **60**, 183.

CHEN, B. & SAFFMAN, P. G. 1980 Steady gravity–capillary waves on deep water. II. Numerical results for finite amplitude. *Stud. Appl. Maths* **62**, 95.

CHOI, I. 1977 Contributions a l'étude des mechanisms physiques de la generation des ondes de capillarité–gravité à une interface air–eau. Thèse, Université d'Aix Marseille.

COHEN, L. S. & HANRATTY, T. J. 1965 Generation of waves in the concurrent flow of air and liquid. *AIChE J.* **11**, 138.

DRAZIN, P. G. 1970 Kelvin–Helmholtz instability of finite amplitude. *J. Fluid Mech.* **42**, 321.

HANRATTY, T. J. 1983 Interfacial instabilities caused by air flow over a thin liquid layer. *Waves on Fluid Interfaces*. Academic.

KAWAI, S. 1979 Generation of initial wavelets by instability of a coupled shear flow and their evolution to wind waves. *J. Fluid Mech.* **93**, 661.

KORDYBAN, E. S. & RANOV, T. 1970 Mechanism of slug formation in horizontal two-phase flow. *J. Basic Engng* **92**D (4), 857.

LIN, P. Y. & HANRATTY, T. J. 1986 Prediction of the initiation of slugs with linear stability theory. *Intl J. Multiphase Flow* **12**, 79.

MASLOWE, S. A. & KELLY, R. E. 1970 Finite amplitude oscillations in a Kelvin–Helmholtz flow. *Intl J. Non-Linear Mech.* **5**, 427.

MILES, J. W. 1957 On the generation of surface waves by shear flows. *J. Fluid Mech.* **3**, 185.

MILES, J. W. 1959 On the generation of surface waves by shear flows. Part 3: Kelvin–Helmholtz instability. *J. Fluid Mech.* **6**, 583.

MILES, J. W. 1986 Weakly nonlinear Kelvin–Helmholtz waves. *J. Fluid Mech.* **172**, 513.

NAYFEH, A. H. & SARIC, W. S. 1972 Nonlinear waves in Kelvin–Helmholtz flow. *J. Fluid Mech.* **55**, 311.

PIERSON, W. J. & FIFE, P. 1961 Some nonlinear properties of long-crested periodic waves with lengths near 2.44 centimeters. *J. Geophys. Res.* **66**, 163.

PULLIN, D. I. & GRIMSHAW, R. H. J. 1983 Nonlinear interfacial progressive waves near a boundary in a Boussinesq fluid. *Phys. Fluids* **26**(4), 897.

RAMAMONJARISOA, A., BALDY, S. & CHOI, I. 1978 Laboratory studies of wind-wave generation, amplification and evolution. In *Turbulent Fluxes through the Sea Surface, Wave Dynamics and Prediction*. Plenum.

SAFFMAN, P. G. & YUEN, H. C. 1982 Finite-amplitude interfacial waves in the presence of a current. *J. Fluid Mech.* **123**, 459.

SCHWARTZ, L. W. & VANDEN-BROECK, J.-M. 1979 Numerical solution of the exact equations for capillary–gravity waves. *J. Fluid Mech.* **95**, 119.

TAITEL, Y. & DUKLER, A. E. 1976 A model for predicting flow regime transitions in horizontal and near horizontal gas–liquid flow. *AIChE J.* **22**, 47.

VANDEN-BROECK, J.-M. 1980 Numerical calculation of gravity–capillary interfacial waves of finite amplitude. *Phys. Fluids* **23**(9), 1723.

WALLIS, G. B. & DOBSON, J. E. 1973 The onset of slugging in horizontal stratified air–water flow. *Intl J. Multiphase Flow* **1**, 173.

WEISSMAN, M. A. 1979 Nonlinear wave packets in the Kelvin–Helmholtz instability. *Phil. Trans. R. Soc. Lond.* A**290**, 639.

WILTON, J. R. 1915 On ripples. *Phil. Mag.* **29**, 688.